Research Square

Preprints are preliminary reports that have not undergone peer review.
They should not be considered conclusive, used to inform clinical practice,
or referenced by the media as validated information.

Integrated Gravity–Magnetic Interpretation for Litho-Structural Mapping and Mineralisation Targeting in the Eastern Part of Son Valley Region, Central India

GAUTAM KUMAR

gautamgp15@gmail.com

Geological Survey of India Northern Region https://orcid.org/0000-0003-4578-0082

Tashmeet Kaur

Geological Survey of India Northern Region

Apratim Kumar Rai

Geological Survey of India

Shahina Siddiqui

Geological Survey of India Northern Region

Resmi Sathikumar

Geological Survey of India Northern Region

Utkarsh Tripathi

Geological Survey of India Northern Region

Research Article

Keywords: Gravity, Magnetic, Son–Narmada Lineament, Mahakoshal, Mineral prospectivity, Lineament analysis, 2D modelling

Posted Date: July 30th, 2026

DOI: https://doi.org/10.21203/rs.3.rs-10344585/v1

License: This work is licensed under a Creative Commons Attribution 4.0 International License.
Read Full License

Integrated Gravity–Magnetic Interpretation for Litho-Structural Mapping and Mineralisation Targeting in the Eastern Part of Son Valley Region, Central India

Gautam Kumar[*1], *Tashmeet Kaur*[1], *Apratim Kumar Rai*[1], *Shahina Siddiqui*[1], *Resmi Sathikumar*[1], *Utkarsh Tripathi*[1]

[1] *Geological Survey of India, Northern Region, Aliganj, Lucknow-226024, India,*

**corresponding author: Gautam Kumar,* ORCID :0000-0003-4578-0082

Gautam Kumar: gautamgp15@gmail.com

ABSTRACT

The Eastern Son Valley of Central India represents a tectonically complex region comprising the Archean basement, Proterozoic Mahakoshal Belt, Vindhyan Supergroup, and Gondwana sediments. This study integrates gravity and magnetic data to delineate lithological boundaries, subsurface structures, and prospective mineralisation zones. Magnetic data were processed using reduction to the pole (RTP), analytic signal, first vertical derivative, and tilt derivative, while gravity data were analysed through regional–residual separation, upward continuation, and derivative techniques. The Bouguer gravity and RTP magnetic anomaly maps reveal prominent ENE–WSW to E–W trending structural features associated with basement heterogeneity, major fault systems, and mafic intrusions. Derivative maps delineate the Son–Narmada North Fault (SNNF), Son–Narmada South Fault (SNSF), and associated structural corridors controlling lithological contacts and intrusive emplacement. Depth estimation using spectral analysis, Euler deconvolution, and PDepth indicates source depths ranging from shallow (<1 km) to deep crustal levels (~8 km). Integrated 2.5D GM-SYS modelling successfully constrains the subsurface geometry, identifying dense and highly magnetic metabasic, ultramafic, and BIF bodies emplaced within the granitic basement. The structurally disturbed corridor between the SNNF and SNSF is interpreted as the most favourable zone for concealed mineralisation. Seven prospective target blocks (A–G) were delineated, demonstrating the effectiveness of integrated potential-field analysis for litho-structural mapping and mineral exploration in Precambrian shield terrains.

Keywords: Gravity, Magnetic, Son–Narmada Lineament, Mahakoshal, Mineral prospectivity, Lineament analysis, 2D modelling

1. Introduction:

The Central Indian Craton preserves a complex record of Precambrian geological evolution, comprising Archean crystalline basement, Proterozoic mobile belts, and overlying sedimentary basins (Naqvi & Rogers, 1987; Ramakrishnan & Vaidyanadhan, 2010). Among these, the Mahakoshal Group, Bundelkhand–Dudhi granitoids, and the Vindhyan Supergroup represent distinct tectono-stratigraphic domains formed under varying geodynamic conditions (Srivastava, 2012; GSI, 2011).

The Son Valley region occupies a critical transitional zone within this framework, where Archean to Proterozoic basement rocks are overlain by thick sedimentary successions and intruded by granitoids and mafic bodies (GSI, 2006; Mishra et al., 2000). This region is structurally controlled by the ENE–WSW trending Son–Narmada Lineament (SNL), a major intracratonic feature that has undergone multiple phases of reactivation since the Precambrian (Ravi Shankar, 1991; Tiwari et al., 2001). The lineament has played a significant role in controlling sedimentation, magmatism, and deformation, influencing the development of the Vindhyan and Gondwana basins as well as the emplacement of younger igneous rocks (Choubey et al., 1999; Mahadevan, 2002).

The presence of structurally controlled mineralization, particularly gold within the Mahakoshal belt, further enhances the geological significance of the region (Saha et al., 2011). Given this complexity, the Son Valley sector provides an ideal natural laboratory for integrated geological and geophysical investigations aimed at understanding crustal architecture, tectonic evolution, and mineralisation processes.

The study area covers about 11,000 km2 in parts of Sonbhadra and Chandauli districts of Uttar Pradesh, Sidhi district of Madhya Pradesh, Sarguja and Korea districts of Chhattisgarh, Garhwa district of Jharkhand and Kaimur district of Bihar, located between 23 ° 45’ N and 24 ° 45’ N and 82 ° 30’ E and 83 ° 30’ E (Figure-1).

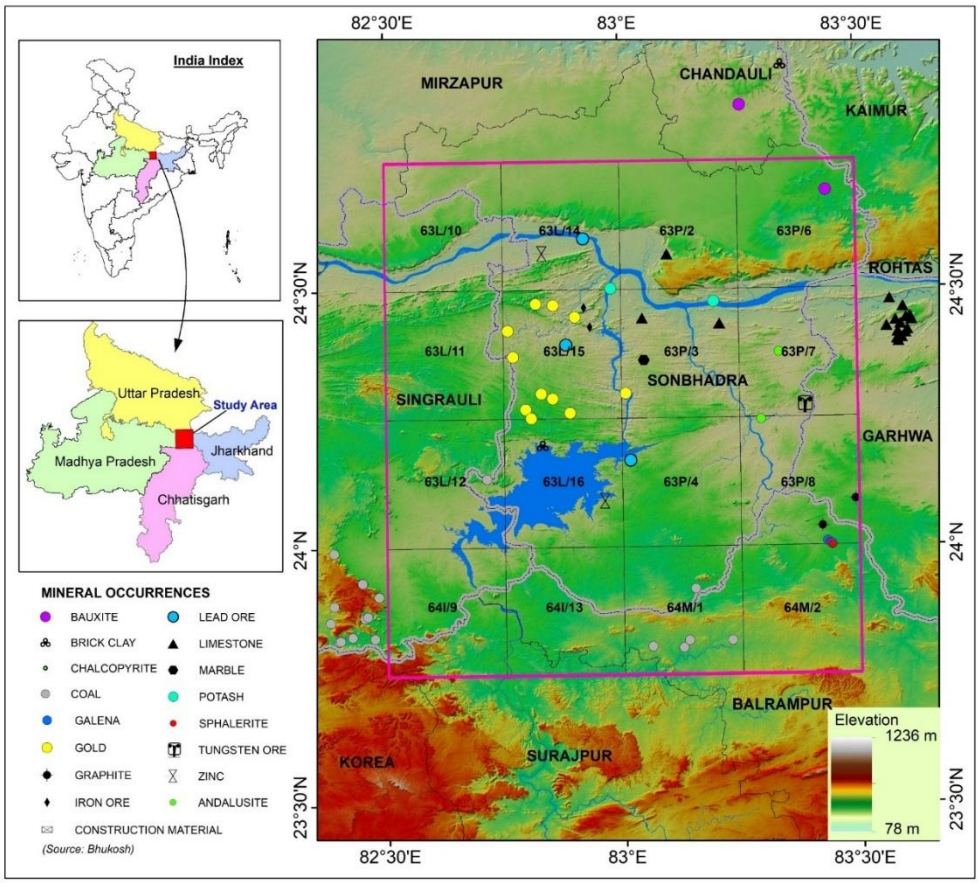


Figure-1: Location map of the study area

This study aims to bridge this gap and provide a complete subsurface model of the region. The objectives of the studies are: (1) Delineate major structural features (faults, shear, contacts) from processed gravity and magnetic data. (2) Correlate geophysical anomalies with known mineralisation and identify new prospective zones. (3) Develop 2D density and susceptibility models of the subsurface. (4) Propose a tectonic and mineralization model for the region.

2. Geological setting:

Regionally, the Mahakoshal Fold Belt forms a prominent E–W to ENE–WSW trending linear zone along the Son–Narmada Lineament (Ramakrishnan & Vaidyanadhan, 2010). It is bounded by the Son–Narmada North Fault (SNNF) in the north and the Son–Narmada South Fault (SNSF) in the south. The SNNF separates the Mahakoshal belt from the relatively undeformed Proterozoic Vindhyan Supergroup and the Sidhi Gneissic Complex, while the SNSF marks the boundary with the granites and gneisses of the Chhotanagpur Gneissic Complex and Gondwana sedimentary sequences (GSI, 2006; Srivastava, 2012).

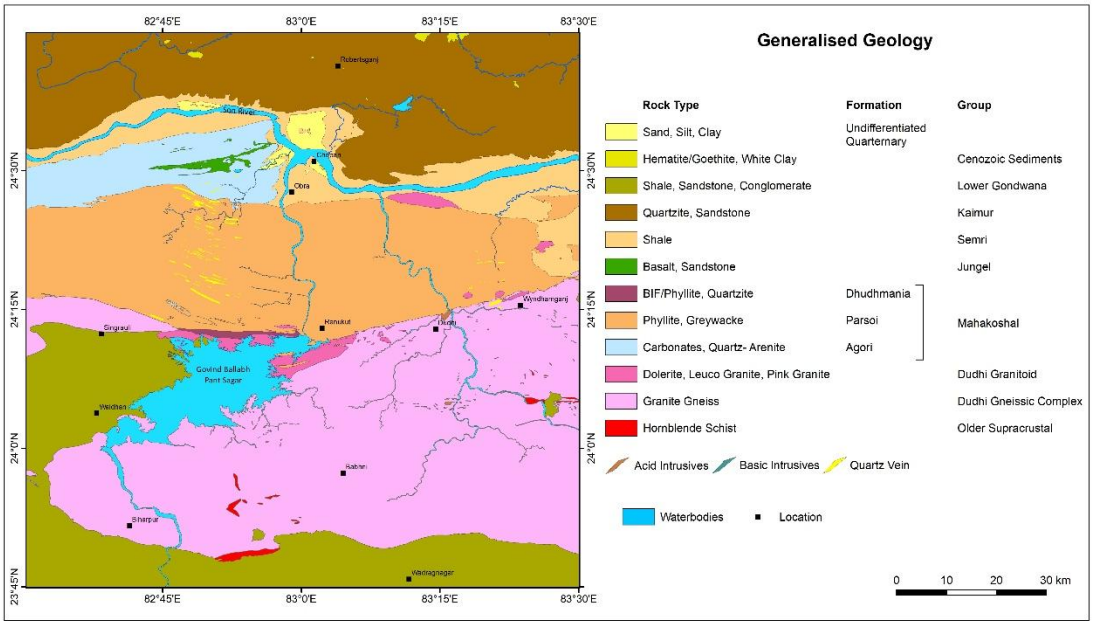


Figure-2: Geological Map of the Study Area ((Source: GSI 1:50000 map series)

The study area comprises lithological units ranging in age from Archean to Quaternary, including the Dudhi Gneissic Complex, Mahakoshal Group, Vindhyan Supergroup, Gondwana Supergroup, and recent alluvial deposits (Figure-2).

The **Dudhi Gneissic Complex**, representing the Archean basement, consists predominantly of granitic gneisses and granitoids such as biotite granite, porphyritic granite, and banded gneiss, with localized occurrences of unakite (GSI, 2006). These rocks form the crystalline basement upon which younger sequences were deposited. The **Mahakoshal Group**, of Palaeoproterozoic age, represents a volcano-sedimentary sequence developed in a tectonically active mobile belt (Ramakrishnan & Vaidyanadhan, 2010). It is subdivided into the Agori, Parsoi, and Dudhmaniya Formations. The Agori Formation comprises basic volcanic rocks, tuffs, ash beds, crystalline limestone, banded iron formations (BHQ/BHJ), phyllite, and shale, intruded by quartz veins and dolerite dykes (GSI, 2011). The Parsoi Formation consists mainly of interbedded phyllite, slate, and quartzite, with localized development of andalusite-bearing phyllite and mica schist near granitic intrusions. The Dudhmaniya Formation includes interbedded phyllite, slate, quartzite, banded iron formations, and mica schist, often associated with younger intrusives (Srivastava, 2012). Gold mineralization, both as sulphides and native gold, has been reported from sheared zones within the Agori and Parsoi Formations (Saha et al., 2011). The **Vindhyan Supergroup**, of Mesoproterozoic age, unconformably overlies the Mahakoshal rocks and represents a relatively stable intracratonic sedimentary basin (Choubey et al., 1999; Mahadevan, 2002). It comprises the Semri and Kaimur Groups. The Semri Group includes formations

characterised by sandstone, orthoquartzite, limestone, porcellanitic shale, and carbonaceous shale with well-preserved sedimentary structures such as ripple marks and stromatolites. The overlying Kaimur Group consists predominantly of quartz arenite, ferruginous sandstone, conglomerates, shale, and laterite (GSI, 2011). The **Gondwana Supergroup** is represented by the Talchir and Barakar Formations, deposited in fault-controlled basins associated with reactivation of the Son–Narmada Lineament (Mahadevan, 2002; Tiwari et al., 2001). The Talchir Formation includes boulder beds, shale, and sandstone, while the Barakar Formation comprises feldspathic sandstone, carbonaceous shale, fireclay, and coal seams. Quaternary sediments, consisting of unconsolidated sand, silt, and clay, occur mainly in the northern part of the study area and are classified into Older and Newer Alluvium (GSI, 2006).

Structural Framework

The structural architecture of the study area is dominated by the Son–Narmada Lineament system and its associated faults and shear zones, which collectively define the tectonic grain of the region (Ravi Shankar, 1991; Tiwari et al., 2001). The **Son–Narmada North Fault (SNNF)** forms the northern boundary of the Mahakoshal belt and marks the contact with the Vindhyan Supergroup. It trends NE–SW and dips steeply towards the northwest. The Vindhyan strata adjacent to the fault exhibit folding, with fold intensity decreasing away from the fault, indicating its strong tectonic influence (GSI, 2006). The **Son–Narmada South Fault (SNSF)** constitutes the southern boundary and is expressed as a major shear zone affecting granitic rocks. This zone is characterized by mylonitic foliation, stretching lineation, mesoscopic folds, and shear bands, indicating intense ductile deformation and repeated reactivation (Ramakrishnan & Vaidyanadhan, 2010). The Amsi–Jiyawan Fault marks the boundary between volcanic-bearing supracrustals and non-volcanic clastic sequences within the Mahakoshal Group. Although the fault plane is not directly exposed, it is inferred from lithological juxtaposition and structural relationships. The occurrence of a quartz reef along its trace, showing evidence of ductile deformation followed by brittle fracturing, suggests a long-lived structural feature, possibly syndepositional in origin (Srivastava, 2012).

Overall, the region is characterised by ENE–WSW–trending structural elements, including faults, shear zones, and lineaments, which have played a critical role in controlling sedimentation, deformation, magmatism, and mineralisation. These structures also act as conduits for fluid migration and are therefore of prime importance in geophysical interpretation and mineral exploration.

3. Data and Methodology:

3.1 Data Source: The Gravity and Magnetic data collected by the Geological Survey of India (GSI) under Project National Geophysical mapping (NGPM) with CG–5 gravimeter (measurement accuracy: 0.001 mGal), GSM–19TW Proton Precession Magnetometer (accuracy: 0.1 nT), and Leica DGPS (vertical accuracy: 5–10 mm in different phases is compiled and used in present study (Source: https://bhukosh.gsi.gov.in/Bhukosh/Public). The data was collected with an average station density of 2.5 square kilometres (figure-3) in the accessible area. The gravity data was reduced to mean sea level after applying elevation correction. Bouguer gravity anomaly over the study area was computed for mean crustal density of 2.67gm/cc. For latitude correction, international gravity formula 1980 was used. The magnetic survey was carried out at the same stations as the gravity measurements. The field magnetic data were subjected to diurnal correction and International Geomagnetic Reference Field (IGRF) correction for calculating magnetic anomalies.

3.2 Methodology: To investigate the subsurface architecture and structural framework of the eastern Son Valley region, the gravity and magnetic data were jointly interpreted. The non-uniformly distributed measurement points were first interpolated onto a regular 500 m grid using a minimum curvature algorithm. This process generated the Bouguer anomaly map and magnetic anomaly map used in the subsequent analysis. The magnetic data were transformed using the Reduction to the Pole (RTP) technique (Baranov, 1957) to centre anomalies over their causative sources. This process corrects for the inclination and declination of the Earth's magnetic field and is a critical step before joint interpretation with gravity data.

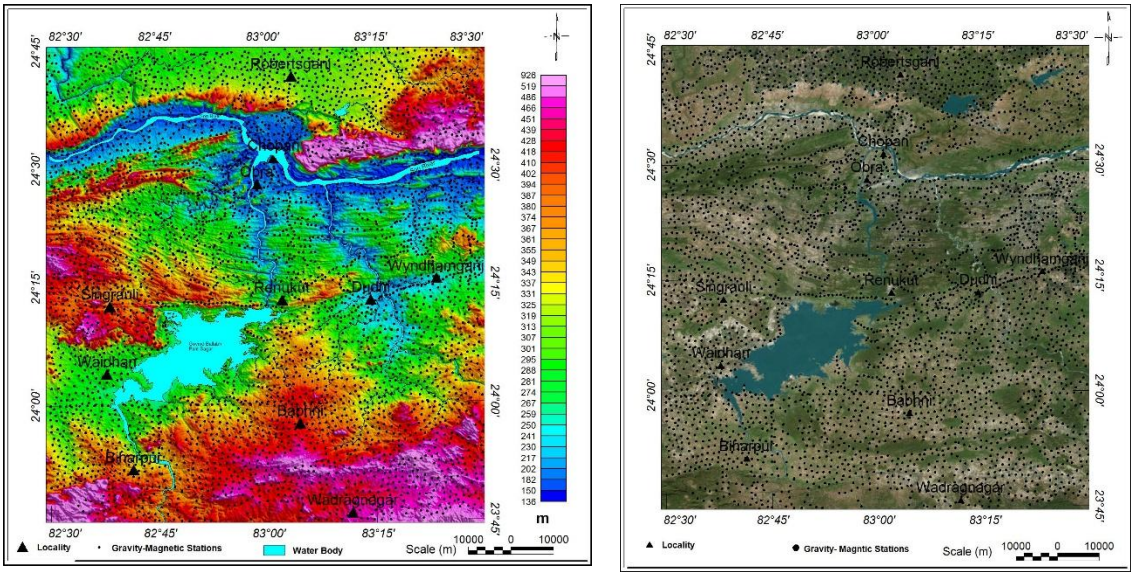


Figure-3: Topographic Map of the study area (a) SRTM Grid (b) Azure Map. Black dots represent gravity and magnetic stations (GSI) (https://bhukosh.gsi.gov.in/Bhukosh/Public

3.3 Regional- Residual separation: Gravity and magnetic anomalies represent composite signals from multiple subsurface sources at varying depths. To isolate these contributions, regional-residual separation techniques such as wavelength filtering, polynomial fitting, and continuation methods are commonly employed (e.g., Spector and Grant, 1970; Jacobsen, 1987; Telford et al., 1990). In this study, upward continuation was selected to generate the regional gravity and magnetic fields. This filter attenuates short-wavelength, near-surface noise while enhancing the long-wavelength signatures of deeper crustal structures. The corresponding residual anomaly maps—highlighting the signatures of shallower geological features—were then calculated by subtracting the upward-continued regional grids from the original Bouguer gravity anomaly (BA) and total magnetic intensity (MA) grids.

3.4 Derivative Analysis: Analysis of the spatial gradients of the potential field data is a common approach for studying shallow gravity- magnetic anomalies. By emphasising subtle changes in the potential field, such derivative analysis improves the identification and characterisation of subsurface structures. Several methods based on estimating vertical $\frac{\partial f}{\partial z}$ and horizontal $\left(\frac{\partial f}{\partial x}, \frac{\partial f}{\partial y}\right)$ gradients of potential field data have been developed for determining the geometric parameter of causative bodies (such as the location and depth of boundaries) and structures (e.g., major faults, magmatic intrusions, salt domes) (e.g., Nabighian, 1972; Ravat et al., 2002; Roest et al., 1992). We calculated four gravity field derivatives: the first vertical derivative, the total horizontal derivative (THDR), the analytical signal (AS), and the tilt angle (TA). Similarly, three field derivatives were calculated for magnetic data: Analytic signal (AS), First vertical derivative of RTP map and Tilt angle of the RTP map.

The THDR enhances shallow-seated geological features (e.g., geological boundaries, magmatic intrusions, faults, lateral lithology variations) while diminishing deeper-seated structures (Fedi & Florio, 2001).

$$THDR = \sqrt{\left(\frac{\partial f}{\partial x}\right)^2 + \left(\frac{\partial f}{\partial y}\right)^2}$$

The THDR highlights steep gradients across abrupt horizontal lithological and structural changes, serving as an edge detector (Cooper & Cowan, 2008; Cordell etal., 1985). However, depth constraints on such contacts are lost (Nishijima & Naritomi, 2017). It is noteworthy that when interpreting horizontal gradients, maxima may not align directly with boundary locations if the boundaries are not vertical or closely spaced (Grauch & Cordell, 1987).

The AS is a complex-valued function representing the combined effects of the vertical and horizontal gradients (Blakely, 1996; Nabighian,1972,1974).

$$AS = \sqrt{(\partial f/\partial x)^2 + (\partial f/\partial y)^2 + (\partial \mathrm{f}/\partial z)^2}$$

Similar to THDR, the AS reveals maxima above near-vertical density contrasts, but tends to smooth high frequency noise (Nabighian,1972; Roest etal.,1992).

The TA is an edge detection method based on the relation between vertical derivative and horizontal derivative data (Ferreira et al., 2013):

$$TA = \arctan\left(\frac{\partial f/\partial z}{THDR}\right)$$

The TA displays balance maxima over the edges of sources at different depths or for superimposed sources (Alhassan et al., 2021; Ferreira et al.,2013)

3.5 Depth Analysis: Depth estimation from potential field data is a fundamental step in quantifying the geometry and subsurface distribution of causative bodies. In this study, depth to source analysis of the Bouguer gravity and magnetic anomalies was performed using Euler 3D deconvolution (Reid et al., 1990; Thompson, 1982) and spectral analysis (Spector and Grant, 1970). For spectral analysis, the radially averaged power spectrum (RAPS) method (Mishra and Pedersen, 1982) was applied. The power spectra were interpreted as comprising distinct linear segments, the slopes of which were determined via least-squares fitting. The average depth to the top of sources for each segment was subsequently calculated by dividing the slope by 4π, delineating shallow, intermediate, and deep crustal source levels.

The Euler 3D depth solution is a technique applied to gridded potential field data to determine the position, depth and nature of any sources (Reid et al, 1990). The Euler deconvolution technique uses first-order x, y and z derivatives to determine location and depth for various idealized targets, each characterized by a specific structural index using Euler′s relation for homogeneous function (Thompson, 1982). The 3D Euler deconvolution method of Reid et al. (1990) is widely used to determine depth persistence and subsurface locations of causative source for discrete gravity anomalies on the basis of gradient of potential field.

The depth of the source body is determined by solving the equation as given by

$$(x - x_0)\frac{\partial f}{\partial x} + (y - y_0)\frac{\partial f}{\partial y} + (z - z_0)\frac{\partial f}{\partial z} \quad = -N(\mathrm{B} - \mathrm{f})$$

Where, x0, y0 and z0 are the position of the source body, which produces the potential field f at coordinate (x, y, z) and N indicates the structural index and B is the back ground field. Euler solutions are particularly used for delineating the horizontal and vertical contacts, depth and nature of causative source. Euler depth solutions has been performed with Structural Index (SI)= 0 and window length (10) for gravity data and Structural Index (SI)= 1 and window length (10) for magnetic data to derive depth solutions for causative body.

4 Results

4.1 Bouguer Anomaly (BA) Map and its Geological Implications:

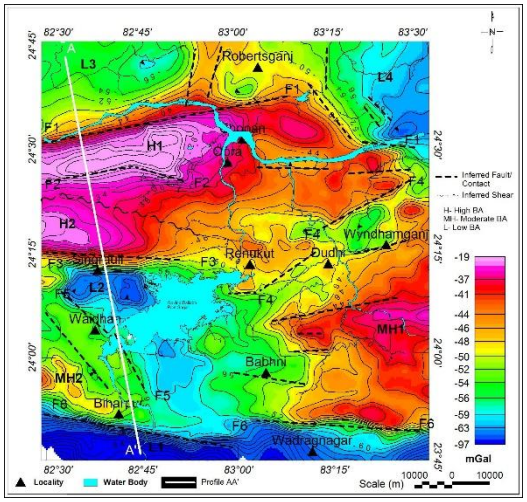


Figure-4.1a: Bouguer anomaly (BA) map of the study area.

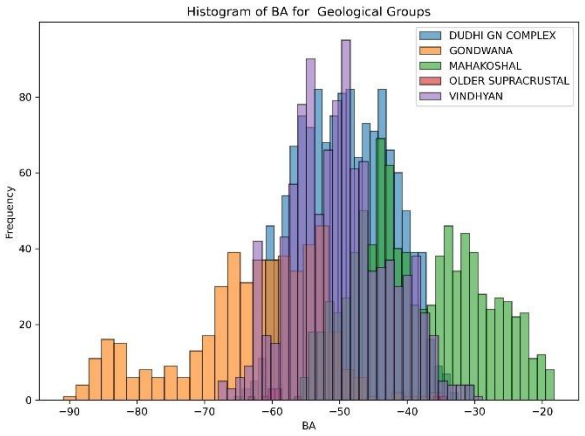


Figure-4.1b: Distribution of BA Values across Geological Groups in the study area

An overall Bouguer anomaly variation of about 78 mGal is observed in the study area (Figure 4a), with values ranging from a minimum of −97 mGal to a maximum of −19 mGal. The anomaly pattern shows a predominant ENE–WSW to E–W trend, which broadly conforms to the regional strike of the geological formations in the area. The Bouguer anomaly (BA) map exhibits relatively high values (H1 and H2) over the ENE–WSW trending linear Mahakoshal formations. Moderate BA values (MH1) are observed over the Dudhi Granite Complex. Low BA values (L1 and L2) characterise the Gondwana formations, while very low BA values (L3 and L4) are associated with the Vindhyan formations. The prominent Bouguer anomaly highs (H1 and H2) are attributed to the presence of high-density volcano-sedimentary rocks and mafic to ultramafic intrusives within the Mahakoshal Group. These anomalies may also be related to horst structures or basement uplift within the Mahakoshal terrain. A broad gravity high has been observed north-east of Chopan, indicating the extension of Mahakoshal rocks below Vindhyan sediments. The gravity field gradually decreases towards the south with moderate gravity NE of Renukut and north of Wyndhamganj areas are due to thinning of the Mahakoshal sequence and lower density of granite and Dudhi granitoid. The low Bouguer anomaly values L1 and L2, ranging from −56 mGal to −97 mGal, and L3 and L4, ranging from −50 mGal to −65 mGal, reflect thick accumulations of low-density Gondwana and Vindhyan sediments, respectively. These zones may correspond to structural depressions or graben-like features, indicating basin development and sediment infill. The moderate gravity high MH-I in over granite gneisses is due to densification of gneisses by high-grade metamorphism or due to a basic intrusive body. A localised moderate anomaly (MH2) within the Gondwana terrain may indicate the presence of comparatively high-density rocks in the subsurface.

The sharp gravity along the ENE–WSW direction indicates a major lineament /fault (F1–F1) represent the southern boundary of the Vindhyan basin and the northern boundary of the Mahakoshal belt. F1–F1 seems to be extended further towards the eastern side with NW- SE orientation in the subsurface; it is part of the Son–Narmada North Fault (SNNF). Another high gravity gradient trending ENE–WSW direction (F2-F2) running further east within Mahakoshal infers a deep-seated contact and represent the Jiawan–Amsi . In the central part of the area, the steep gravity gradient trending E–W to NE-SW marked as F3–F3 and F4-F4, marks the southerly dipping steep fault boundary between Mahakoshals and Gondwana and Mahakoshals and Dudhi Granitoids, respectively. It is to be a part of the Son–Narmada South Fault (SNSF). Regionally, the northern and southern boundaries of Mahakoshal constitute the Son Narmada Fault System. Another E-W trending steep gravity gradient in the southern part (F6-F6) represent the contact between Dudhi Granitoid, older Supracrustal and Gondwana Sediment. The inferred lineaments/ contacts obtained from BA anomalies show that most of the lineaments/ contacts are oriented E–W, ENE–WSW, NW-SE and N–S directions. In the central part of the area, a curvilinear low BA nosing is observed, which is characterised by the shear zone within Mahakoshal.

The histogram of Bouguer Anomaly (BA) values (Figure-4b) shows clear lithological control on density distribution across the geological groups. The Gondwana formations exhibit very low BA values (−90 to −55

mGal), indicating low-density sedimentary sequences, whereas the Vindhyan group shows moderately higher values (−65 to −45 mGal), reflecting relatively compact platform sediments. In the study area, Gondwana basins are structurally down-faulted and thicker, enhancing the gravity low due to increased thickness of low-density sediments, whereas Vindhyan formations are comparatively stable and thinner platform sequences, contributing to relatively higher BA responses. The Dudhi Granite Complex displays a narrow and consistent range (−60 to −40 mGal), characteristic of homogeneous crystalline basement rocks, while the Older Supracrustal units overlap with Vindhyan and Dudhi, suggesting mixed lithology and moderate density contrast. The older supracrustal rock is Hornblende schist. Despite the presence of hornblende, the schistose fabric, deformation, and alteration of the Older Supracrustal rocks reduce their bulk density, resulting in relatively lower Bouguer anomaly values. In contrast, the Mahakoshal Group is distinctly shifted toward higher BA values (−50 to −20 mGal) with a broad spread, indicating the presence of dense lithologies such as banded iron formations and mafic units. Overall, the distribution highlights strong density contrasts between sedimentary basins and mineralized terrains, with Mahakoshal anomalies clearly marking zones of higher density and mineralization potential, demonstrating that BA is an effective parameter for lithological discrimination and exploration targeting. The bimodal BA distribution of the Mahakoshal Group reflects the coexistence of low-density metasedimentary units and high-density iron-rich/mafic bodies, indicating significant lithological heterogeneity and mineralisation potential within the belt.

4.1.1 Edge identification and structural analysis from gravity data: The delineation of structural features from gravity data in the study area is achieved through First vertical derivative (1VD), total horizontal derivative (THDR), analytical signal (AS) and Tilt angle analysis (Telford et al., 1990 ; Miller and Singh, 1994 ; Blakely, 1996 ; Pilkington and Keating, 2004 ; Verduzco et al., 2004 ; Rosid and Siregar, 2017). In the present study, these filters were applied to the Bouguer anomaly (BA) data to enhance subsurface structural features and delineate geological boundaries with greater clarity. The THDR and 1VD maps (Figure 4.1.1a and 4.1.1b) effectively emphasise lateral and vertical gradients in the gravity field, respectively, thereby highlighting zones of abrupt density contrast associated with faults, lithological contacts, and lineaments. The THDR map enhances near-surface edges independent of anomaly polarity, while the 1VD sharpens shallow features and suppresses deeper signals. Prominent gradient maxima observed in these maps exhibit preferred orientations along NE–SW, NW–SE, N–S, and E–W directions, reflecting the dominant structural grain and tectonic framework of the study area. These trends likely correspond to multiple phases of deformation and reactivation of pre-existing structural discontinuities. The zero contours of the 1VD map serve as reliable indicators of the edges of causative bodies, marking the transition zones between contrasting density units. These contours effectively delineate shallow subsurface boundaries such as faults, contacts, and fracture zones. Similarly, the analytical signal amplitude (Figure 4.1.1c), which combines both horizontal and vertical derivatives, produces maxima directly over source edges regardless of magnetization or density contrast direction. This makes AS particularly useful in accurately locating structural boundaries, even in complex geological settings.

Furthermore, the tilt angle transformation (Figure 4.1.1d) provides an additional robust means of edge detection by normalizing the signal amplitude. The zero contour of the tilt angle distinctly marks the boundaries of causative sources, while positive and negative values help infer relative depth variations—positive values generally indicating shallow sources and negative values suggesting deeper ones. This attribute enhances the continuity of structural trends and improves the detection of subtle lineaments that may not be clearly visible in other derivative maps.

Overall, the integration of THDR, 1VD, AS, and tilt angle analyses provides a consistent and complementary framework for structural interpretation. The faults, contacts, and lineaments delineated through these methods show strong spatial correlation with those interpreted from the Bouguer anomaly map (Figure 4a), thereby validating the reliability of the applied filtering techniques and reinforcing the inferred structural architecture of the study area.

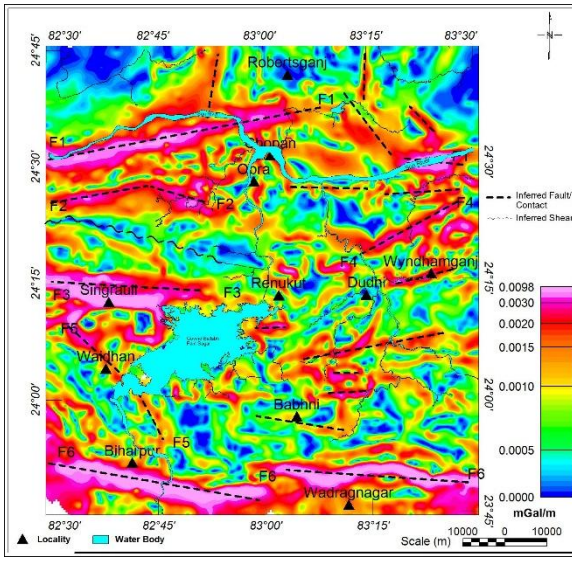


Figure-4.1.1a: *Total horizontal derivative of BA in the study area.*

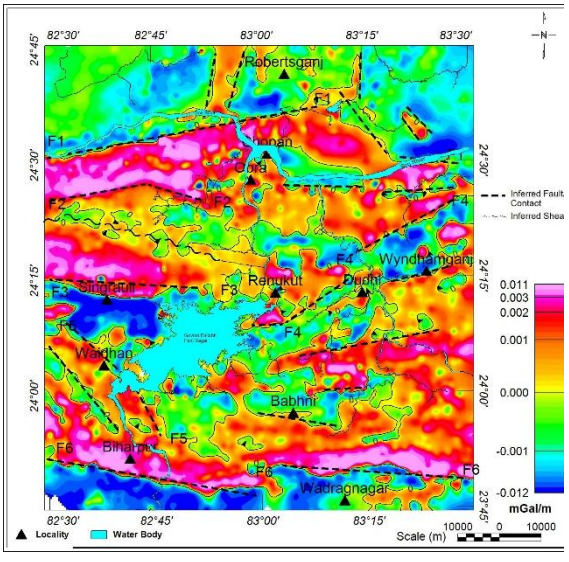


Figure-4.1.1b: *First vertical derivative of BA in the study area.*

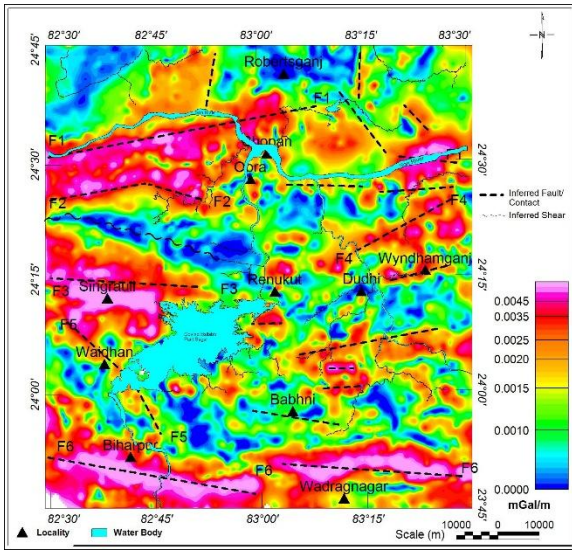


Figure-4.1.1c: *Analytic Signal of BA in the study area.*

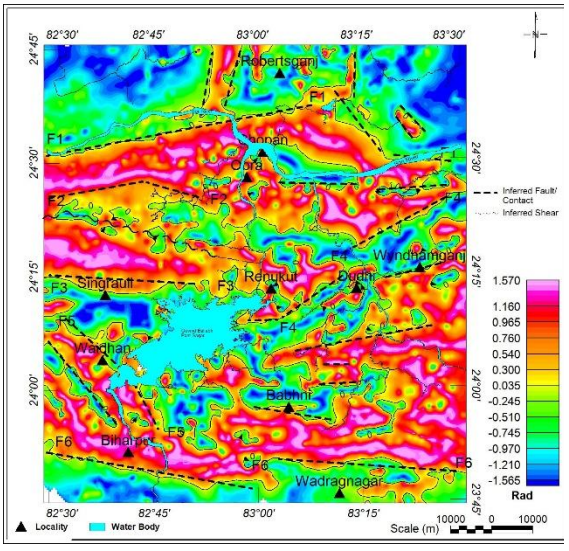


Figure-4.1.1d: *Tilt angle of BA in the study area.*

4.1.2 Regional Gravity Anomaly:

The regional gravity map generated through the upward continuation technique effectively enhances deep-seated structures while attenuating near-surface noise. Upward continuation was carried out at multiple heights of 2, 4, 6, and 8 km (Figure 4.1.2). At lower continuation levels (2–4 km), the gravity gradient exhibits a stepped character, reflecting residual features associated with shallow sources at depths less than 2 km (Figure 4.1.2a, b). In contrast, at higher continuation levels (6–8 km), the gravity anomalies become smoother and more regional in nature, indicating density variations originating from deeper sources, generally below 4 km depth (Figure 4.1.2c, d) (Jacobsen, 1987; Kebede et al., 2020). The upward continued maps reveal that the high Bouguer anomaly (H1) persists even at 8 km, suggesting a deep-seated origin, likely related to high-density mafic to ultramafic rocks within the Mahakoshal Group. Major structural features such as Fault F1 (SNNF), F3, and F4 (SNSF) are distinctly expressed in the 8 km upward continued map, confirming their deep-rooted nature. In contrast, Fault F2 (Jiawan–Amsi) and associated shear zones are well defined up to the 4 km continuation level but gradually lose their expression at higher levels, indicating moderate depth persistence. The high anomaly H2 shows a diminishing trend with increasing continuation height, suggesting a relatively shallow to intermediate depth source, likely controlled by Fault F2 and associated shear zones in the southeastern part of the study area. Furthermore, the persistence of high anomaly H1 along with Faults

F1 and F4 up to the northeastern boundary, followed by their abrupt termination, indicates the probable termination of the SNNF and SNSF structural systems within the study area. Low Bouguer anomaly zones (L1, L3, and L4), which remain prominent across all continuation levels, are indicative of thick accumulations of low-density Gondwana and Vindhyan sediments. The semicircular low anomaly L2 gradually diminishes beyond the 4 km continuation level, suggesting a shallow origin, likely corresponding to Gondwana sedimentary deposits in the vicinity of Singrauli.

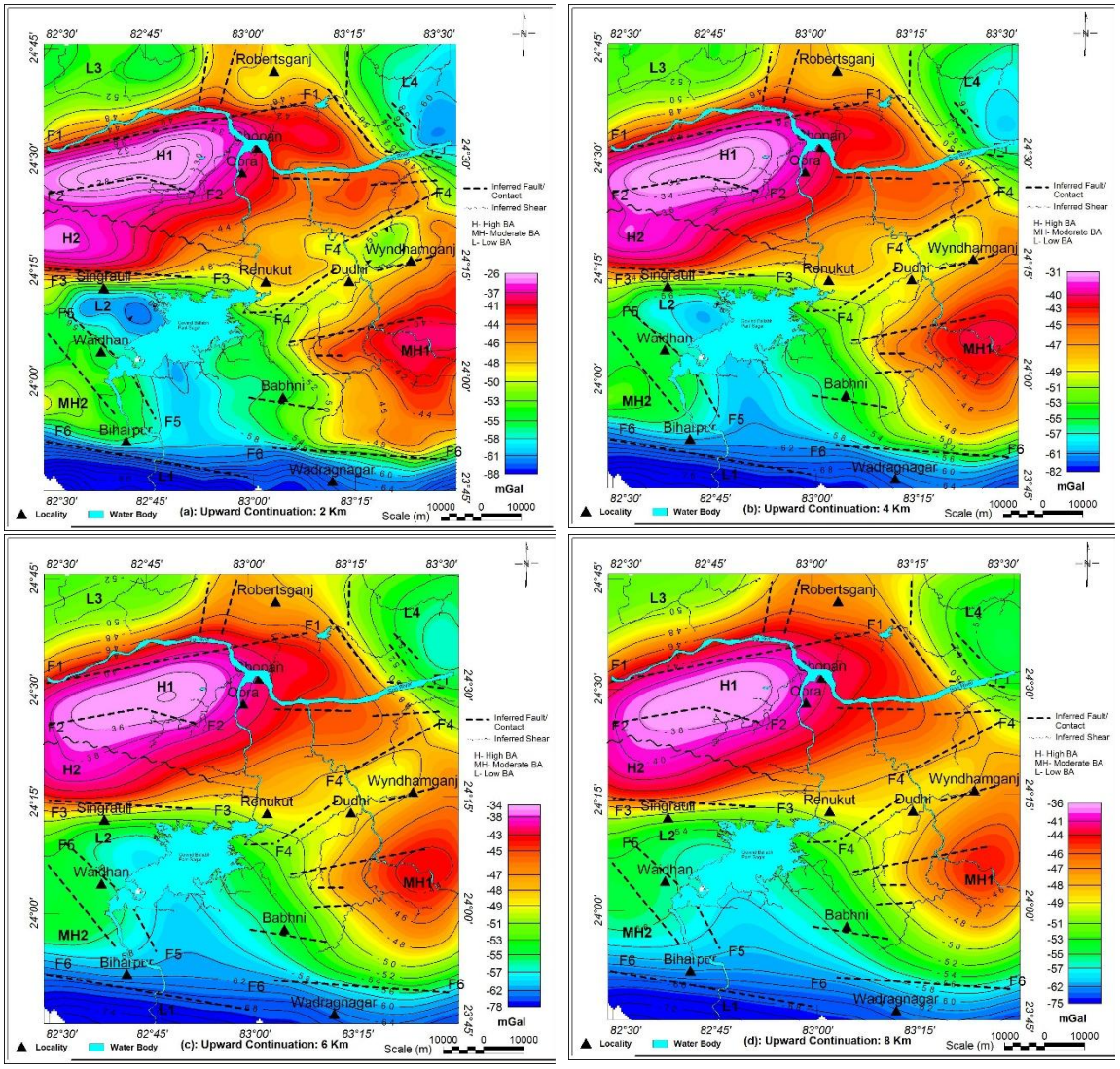


Figure 4.1.2: *Upward continued maps of BA at 2, 4, 6, and 8 km heights in the study area.*

4.1.3 Residual Gravity Anomaly:

The residual gravity map is obtained by subtracting the upward-continued gravity grid at 8 km from the BA grid (Figure 4.1.3). It identifies several residual or near-surface gravity highs (RH1–RH9) and lows (RL1–RL9) across the study area. Residual highs correlate with high–density lithologies such as BIF, amphibolites, and Basic rocks of Mahakoshal. Residual lows are linked to low-density formations, including Gondwana and Vindhyan. Residual Highs (RH1- RH5) are related to high-density rocks of Mahakoshal. While Residual Highs (RH6-RH9) are related to high-density rocks of gneisses or due to basic intrusive body. Residual lows (RL1- RL4) are related to the low-density Vindhyan sediments. RL5-RL6 are due to the presence of granitic rocks in the study area. The Residual Lows RL7-RL9 are due to presence of Gondwana sediment. The distribution of these residual anomalies matches the surface geology revealing localized structural features like faults/contacts and shear zones, particularly trending ENE–WSW, NW–SE, N–S, and E–W. These structures serve as potential zones for mineralisation.

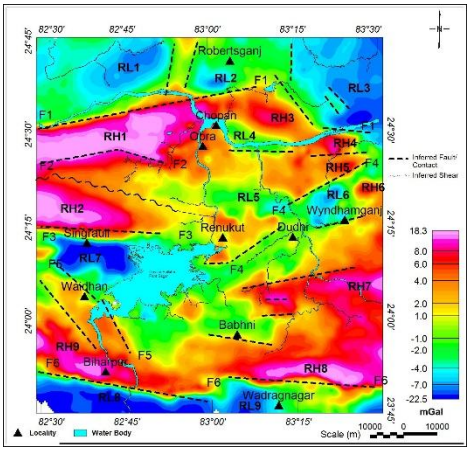


Figure 4.1.3: Residual Gravity anomaly (RHs – residual highs and RLs – residual lows) map of the study Area.

4.2 Magnetic Anomaly (MA) Map and its Geological Implications:

The Total Magnetic Intensity (TMI) map (Figure 4.2a) shows magnetic values ranging from -3113 nT to 2865 nT across the survey area. The map displays a prominent E-W trending magnetic high zone in the central part of the study area, which spatially coincides with the mapped lithounit of the Mahakoshal Group of rock. A low magnetic field is observed in the northern part, representing the Vindhyan sedimentary sequences. Moderate Magnetic anomaly is observed in the southern part, reflecting the presence of Gneissic Basement. The observed magnetic anomaly map shows a characteristic asymmetry as the survey area lies in mid-latitudes (Blakely, 1996). This bipolar asymmetry makes direct geological interpretation difficult and can lead to incorrect positioning of magnetic bodies. The Reduced to Pole (RTP) transformation mathematically repositions the anomalies as if they were measured at the magnetic pole, where inclination is 90° (Grant and West, 1965). This transformation centres the anomalies directly over their sources, removes the north-south asymmetry, and converts dipolar anomalies into monopolar forms that are easier to interpret. Therefore, RTP transformation is essential for accurate delineation of magnetic source boundaries and correlation with geological features in this area. All subsequent interpretations and derivative maps have been prepared using RTP-transformed data to ensure reliable geological correlation.

High magnetic anomalies (MH1, MH2, and MH3) observed in the central part of the study area indicate the presence of magnetite-rich formations, likely Banded Iron Formation (BIF) and Mafic/ultramafic intrusions of the Mahakoshal. Low magnetic zones (ML1, ML3 & ML4) represent sedimentary deposits. Dominant Low anomalies ML1 represent the Vindhyan, while ML3 and ML4 indicate the Gondwana sediment. Low Magnetic zone ML2 observed over the Mahakoshal represents the zone of demagnetisation due to shearing and well-collobrated with the shear zone demarcated from the gravity data. The moderate magnetic high in the southern part reflects the crystalline basement. The Magnetic Lineament (L1-L4) in the central part demarcate the major structural trends/ faults/contact/shear zone. In the study area. The Lineament L1 represents the Son Narmada North Fault (SNNF) and is the contact of Mahakoshal and Vindhyan. The Lineament L4 represents the Son Narmada South Fault (SNSF) and is the contact of the Mahakoshal aand the contact of the Mahakoshal and Dudhi Granitoid in the eastern part. The Magnetic lineament L2 represent the Amsi-Jiyawan Fault, which reflects the formation contact between the Agori formation with associated volcanics and the Parsoi Formation devoid of volcanics. The Lineament L3 reflects the contact between BIF containing Dudhmania formation and Parsoi formation. The Lineament L4 reflects the contact between Mahakoshal and Dudhi Granitoid are attributed to SNSF. The Lineamnet L5 reflect the contact between crystalline basement and Gondwana. Overall the map reveals structurally controlled, shallow magnetite-rich bodies in the central region, separated from a weakly magnetic sedimentary basin in the north and south by major tectonic lineaments.

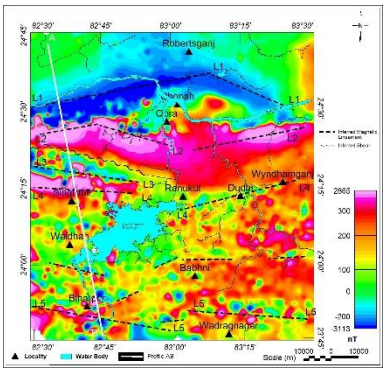


Figure-4.2a: *Magnetic (TF) anomaly map of the study area.*

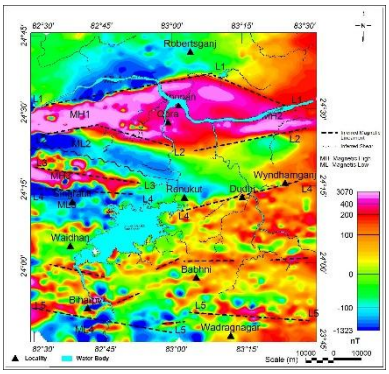


Figure-4.2b: *Reduced to Pole Magnetic map of the study area*

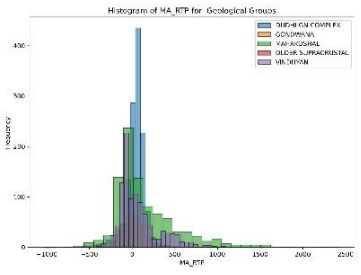


Figure-4.3b: *Reduced to Pole Magnetic map of the study area*

The histogram of magnetic anomaly (MA_RTP) values (Figure 4.3 b) for different geological groups shows a clear distinction in magnetic response among lithologies. The Mahakoshal Group exhibits a strong and highly variable magnetic response in the histogram, characterized by a broad distribution with a noticeable shift toward higher positive MA_RTP values. This reflects the heterogeneous nature of the Mahakoshal lithology, which includes Banded Iron Formation (BIF), mafic volcanics, and metasedimentary units, all contributing to elevated magnetic susceptibility. The widespread and pronounced positive tail indicate the presence of magnetite-rich zones and localized high-intensity anomalies, suggesting shallow and structurally controlled sources. The Dudhi Granitic Complex (DGC) shows a moderate to low magnetic response in the histogram. This suggests that the granitoid rocks of the DGC are weakly to moderately magnetised, consistent with felsic compositions that generally lack abundant ferromagnetic minerals. However, the slight positive skew and occasional higher values indicate localised enrichment of magnetic minerals (e.g., biotite, magnetite, or minor mafic enclaves), possibly due to magmatic differentiation or later alteration. The Gondwana formations show a moderate to low magnetic response in the histogram, with values generally clustered around near-zero to slightly positive MA_RTP. This reflects the dominance of sedimentary lithologies such as sandstones, shales, and coal measures, which are typically weakly magnetic. Magnetic anomalies are subdued due to sedimentary cover masking the basement response. The Vindhyan Supergroup shows a predominantly low to near-zero magnetic response in the histogram, accompanied by a subtle positive tail. This behavior reflects the dominance of weakly magnetic sedimentary rocks such as sandstones, shales, and limestones. The observed positive tail is likely attributable to the influence of underlying Mahakoshal rocks, where shallow or near-subsurface magnetite-bearing units contribute to localized increases in magnetic values beneath the Vindhyan cover.

4.2.1 Edge identification and structural analysis from Magnetic data:

Analytical signal response of the MA, First Vertical derivative of RTP and Tilt angle map further delineated edges of causative bodies, including faults/contacts and lineaments (Figure 4.2.1 a, b & c). AS maxima align with significant structural features such as fault zones, lithological contacts, and serve as potential conduits for mantle–derived materials (Abraham et al., 2024). High-amplitude zones clearly mark sharp lithological contacts, dykes, and intrusive bodies. A prominent E–W to ENE–WSW trending high in the northern part indicates a major structural corridor (L1), representing SNNF. Central and southern areas show discontinuous highs, suggesting fragmented or multiple smaller intrusions/lineaments (L2–L5). The AS map effectively delineates edges of magnetised bodies. The 1VD of RTP enhances near-surface magnetic sources and sharp gradients. Strong alternating positive–negative bands indicate shallow contacts and fault/shear zones. The northern belt again shows a continuous linear high-gradient zone, confirming L1 as a major structural feature. The central region exhibits dense, closely spaced anomalies, indicating intense structural deformation or multiple thin magnetic bodies. Southern part shows linear but relatively subdued gradients, suggesting deeper or less magnetic sources compared to the north. Tilt Angle of RTP is particularly useful for edge detection and depth estimation consistency. The northern sector displays a broad, continuous positive zone, indicating thicker or deeper magnetic bodies. The central part shows alternating narrow bands,

reflecting complex shallow structures and closely spaced lineaments. Linear features corresponding to L1–L5 are more continuous and traceable, making TDR very effective for mapping regional structural trends. The combined analysis of Analytic Signal, First Vertical Derivative, and Tilt Angle maps provides a robust framework for magnetic lineament delineation. A major E–W to ENE–WSW trending lineament (L1) is consistently identified across all maps, indicating a regional-scale fault/contact zone, i.e. SNNF. Secondary lineaments (L2–L5) are observed as discontinuous to semi-continuous features, suggesting fracture zones, minor faults, or dyke swarms. The northern area is dominated by strong, continuous magnetic signatures, implying highly magnetized and structurally controlled lithologies. The central region reflects structural complexity, with dense lineament networks possibly associated with deformation zones/ shear zones or intrusive activity. The southern region shows relatively diffuse and weaker anomalies, indicating deeper or less magnetic basement. Overall, the integration confirms a structurally controlled terrain, where major and minor lineaments likely govern mineralisation pathways and subsurface continuity, relevant for mineralisation targeting in the Mahakoshal belt.

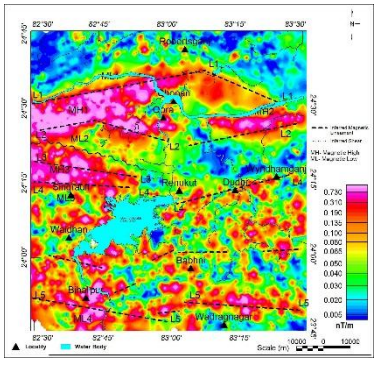


Figure 4.2.1a: *Analytic Signal map of the study area.*

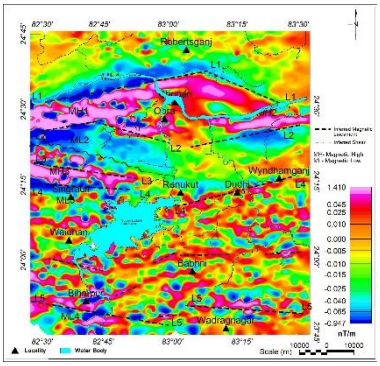


Figure 4.2.1b: *First vertical derivative of RTP in the study area.*

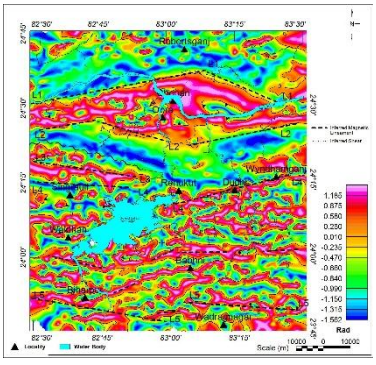


Figure 4.2.1b: *Tilt angle of RTP in the study area.*

4.3 Source depth estimation from gravity and magnetic anomalies:

4.3.1 Radially averaged power spectrum (RAPS) of gravity and Magnetic data

The radially averaged power spectrum (RAPS) of the Bouguer anomaly (Figure 4.3.1a) reveals three major density interfaces at ~8.2 km (D1), ~2.53 km (D2), and ~1.04 km (D3), indicating a vertically stratified crustal structure. The deepest interface (~8.2 km) is interpreted as a major crustal boundary reflecting a significant density contrast within the upper crust. The intermediate depth (~2.53 km) corresponds to the density contrast between the Mahakoshal Group and the underlying granitic–gneissic basement. In contrast, the shallow depth (~1.04 km) reflects near-surface heterogeneities associated with the Vindhyan cover rocks and supracrustal lithological variations. The magnetic RAPS (Figure 4.3.1b) delineates two major susceptibility interfaces at ~2.97 km (S1) and ~1.2 km (S2). The deeper magnetic source (~2.97 km) marks the top of the magnetic basement, attributed to granitic–gneissic crystalline rocks and magnetically active units of the Mahakoshal Group. The shallow magnetic depth (~1.2 km) reflects near-surface magnetic sources such as mafic dykes, banded iron formations, and structurally controlled mineralisation. The correspondence of intermediate depths (~2.5–3 km) in both datasets constrains the basement surface, whereas the absence of a deep magnetic equivalent to the ~8.2 km gravity interface suggests a relatively non-magnetic deeper crust.

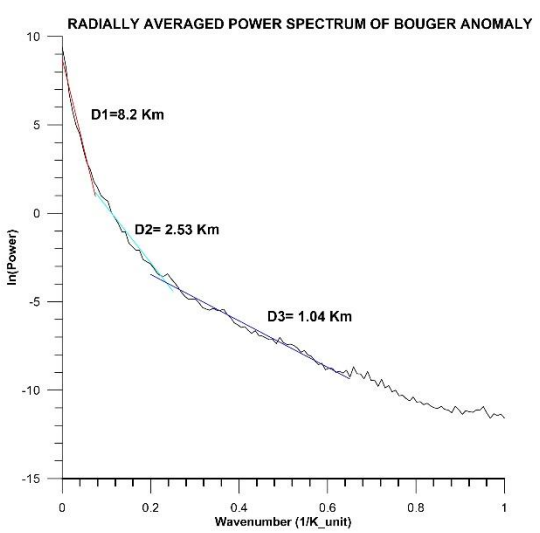


Figure 4.3.1a: Radially averaged power spectrum of gravity data

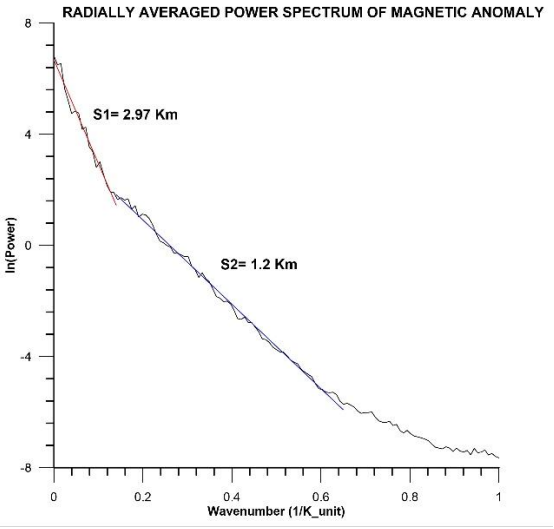


Figure 4.3.1b: Radially averaged power spectrum of magnetic data

4.3.2 Euler 3D depth solutions of gravity and Magnetic data

For the gravity data, most Euler solutions exhibit dominant E–W and ENE–WSW orientations. The solutions are concentrated along the edges of major structures, including F1–F1 (Son Narmada North Fault), Jiawan–Amsi Fault (F2–F2), and SNSF (F3–F3 and F4–F4), as well as along other localised faults and lithological contacts. The linear clustering of solutions along these zones indicates the continuity of faults and contacts at depth. The overall pattern reveals a structurally controlled framework characterised by major E–W trending regional lineaments and cross-cutting NE–SW to NW–SE fractures. The intersection of these structures marks zones of enhanced permeability and potential mineralization. Deeper Euler solutions (~2–4 km) suggest basement-rooted structures that may act as conduits for fluid migration and mineral deposition. For the magnetic data, Euler solutions show dense clustering along high-gradient zones of the analytic signal map, with a similar dominant E–W to ENE–WSW orientation. The strong spatial correspondence between analytic signal highs and Euler solution clusters confirms that these features represent well-defined geological boundaries. These structures are laterally continuous and vertically persistent, extending from near-surface levels down to depths of ~3–4 km**.**

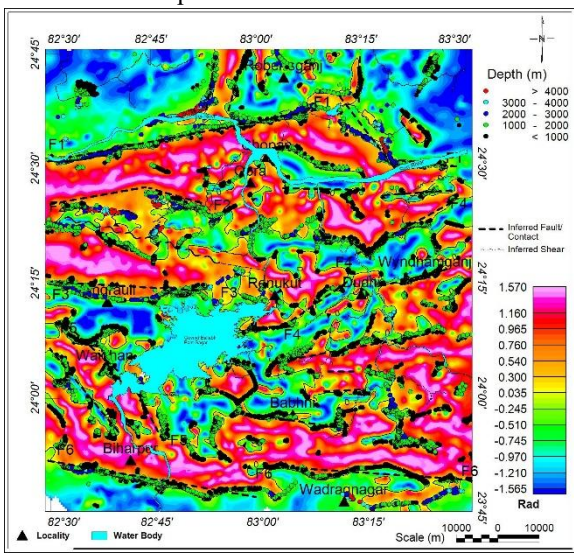


Figure 4.3.2a: Euler 3D solutions of gravity data on the Tilt angle map of BA

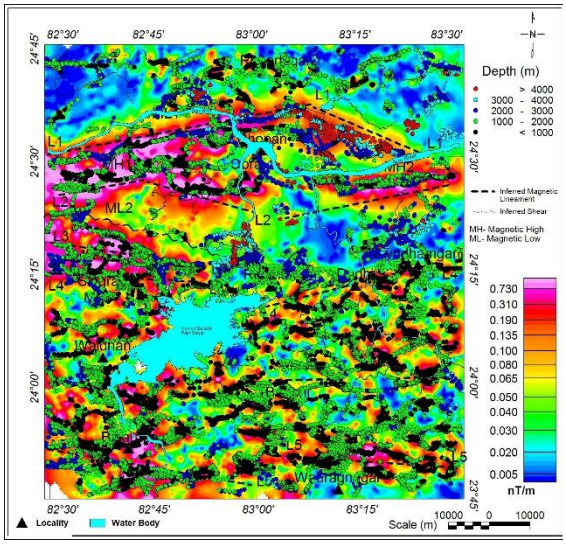


Figure 4.3.2b: Euler 3D solutions of Magnetic data over the analytic signal of MA

5. Geophysical Crustal Modelling:

5.1 1D Analysis from Gravity and Magnetic Data along profile AB

The 1D integrated analysis of gravity and magnetic data along profile AB was carried out to delineate subsurface contacts, faults, shear zones, and intrusive bodies (Figure 5.1a). The profile was oriented approximately perpendicular to the major lithological formations, namely the Vindhyan, Mahakoshal, DGC, and Gondwana sequences, as well as to the dominant structural trends of the area. The integrated interpretation of the Bouguer gravity and RTP magnetic anomalies reveals a structurally complex subsurface architecture characterised by significant lithological contrasts, deep-seated fault systems, basement heterogeneity, and intrusive magmatic activity.

The application of derivative-based enhancement techniques, including horizontal derivative, first vertical derivative, total derivative, and analytic signal analyses, effectively delineates major structural discontinuities and subsurface contacts. Several prominent fault/shear zones identified along the profile are marked as F1, F2, F3, and F6, which correspond to abrupt variations in gravity and magnetic signatures. These structural zones are interpreted as deep-rooted tectonic discontinuities controlling lithological boundaries and magmatic emplacement.

The PDepth (Phillips, 1997), solutions derived from the analytic signal (Nabighian (1972, 1974)) of gravity and magnetic data provide important constraints on the depth extent and geometry of the causative sources. The gravity-derived depth solutions indicate source depths extending up to approximately 5 km, suggesting the presence of deep-seated density interfaces and basement-controlled fault systems. Dense clustering of depth solutions near F1, F2, F3, and F6 indicates major crustal-scale structural corridors that may represent tectonically reactivated fault zones. These structures likely facilitated intrusive emplacement, basement reactivation, and localised basin development. In contrast, the magnetic-derived depth solutions are comparatively shallower, generally extending up to ~4 km, indicating the presence of near-surface magnetic bodies and dyke intrusions. The first vertical derivative (1VD) and total derivative (TD) of RTP anomalies effectively enhance shallow magnetic sources and clearly delineate narrow dyke-like features. A large number of contact and dyke solutions identified between 58 and 90 km along the profile suggest intrusive activity.

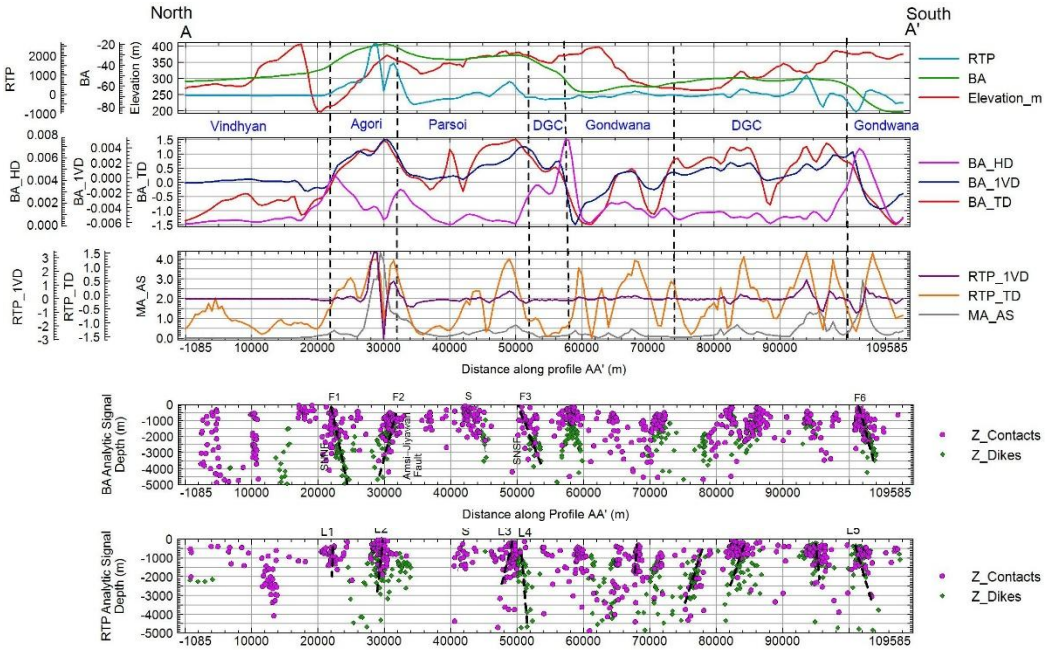


Figure-5.1: 1D analysis of gravity and magnetic data along profile AB. Depth calculated through the Pdepth module using analytic signal from gravity and magnetic data along AB

5.2 Gravity and Magnetic Forward Modelling along profile AB

The crustal architecture of the Eastern Son Basin was investigated along a NNW–SSE-trending 2.5D geophysical profile AB (Figure 4 .1.a and Figure-4.2.a), approximately 110 km in length, using the GM-SYS modelling approach (Figure-5.2). The gravity and magnetic anomaly maps reveal a

prominent ENE–WSW trending feature in the central part of the study area. Accordingly, a NNW–SSE oriented profile (AB), shown on the Bouguer gravity and magnetic anomaly maps, was selected for crustal modelling to intersect the major gravity and magnetic highs. The profile is oriented approximately perpendicular to the regional strike of the major geological units, including the Vindhyan Supergroup, Mahakoshal Group, Dudhi Gneissic Complex (DGC), and Gondwana formations, as well as the major tectonic structures such as the Son–Narmada North Fault (SNNF), Son–Narmada South Fault (SNSF), and Jiawan–Amsi Fault. Modelling of potential field data inherently suffers from non-uniqueness, as a given anomaly can be explained by different combinations of source geometry, depth, and physical properties (Blakely, 1995; Li and Oldenburg, 1996, 1998; Saltus and Blakely, 2011). To reduce this ambiguity, joint gravity and magnetic modelling was carried out, allowing both density and magnetic susceptibility constraints to be applied simultaneously. The model was constrained using surface geological information, geophysical interpretations, and measured density values of rock samples collected during the field survey (Table 1). Forward modelling was performed using the GM-SYS module of Geosoft (version 2025.1). The integrated gravity and magnetic modelling assumes that both anomalies arise from common causative sources at depth. However, gravity and magnetic fields respond differently to subsurface bodies depending on their physical properties and depth of occurrence. Magnetic anomalies, dominated by high-frequency components, are particularly effective in delineating shallow crustal features such as dykes, faults, and intrusive bodies, whereas gravity anomalies provide better constraints on deeper crustal structures and the regional basement configuration. Forward modelling of gravity and magnetic responses was carried out using the polygonal modelling algorithms of Talwani et al. (1959) for gravity data and Talwani and Heirtzler (1964) for magnetic data.The model geometry and physical properties were iteratively refined to obtain a satisfactory agreement between the observed and calculated gravity and magnetic anomalies while maintaining geological consistency. After achieving an acceptable forward model, minor adjustments to selected model parameters were carried out using the joint inversion routine available in GM-SYS. The inversion was employed solely to refine the constrained forward model rather than to derive an unconstrained solution. Thus, the adopted workflow comprised geologically constrained forward modelling followed by limited inversion-based refinement.

Lithology	No. of Samples	Density (Min) g/cc	Density (Max) g/cc	Susceptibility (min) cgs x 10^{-6}	Susceptibility (max) cgs x 10^{-6}
BIF/BHQ/BHJ	7	2.405	3.783	11.2	5923.6
Basic-Mafic-Ultramafic Suite	58	2.318	3.567	1.8	7618.2
Chert	6	2.529	2.821	4.2	4669.8
Ferruginous Phyllite	10	2.397	2.975	2.1	7217
Granite + Granite Gneiss	40	2.436	2.939	2.4	1018.6
Phyllite	119	2.303	2.785	0.4	591
Quartz Vein	43	2.423	2.867	0.2	203.7
Quartzite	15	2.233	3.054	1	128.9
Sandstone	15	2.06	2.94	30	77

Table 1. Density and susceptibility measurement of rock samples.

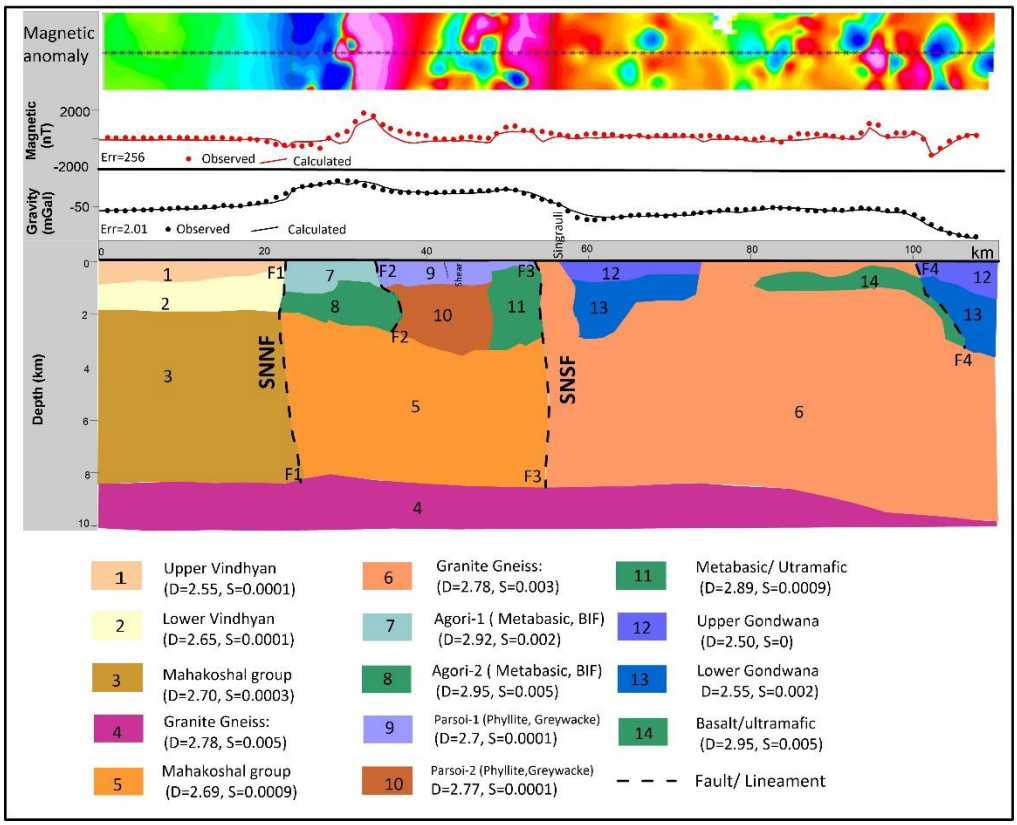


Figure-5.1: 2D Joint gravity and magnetic modelling

The integrated 2.5D GM-SYS model along profile AB successfully reproduces the observed gravity and magnetic anomalies with a close fit between the observed and calculated curves. The model reveals a heterogeneous crust comprising the Vindhyan Supergroup, Mahakoshal Group, granite gneiss, Metabasics/BIF, Parsoi Formation, Gondwana sediments, and Basalt/ultramafic bodies. The shallow Vindhyan sediments overlie the denser Mahakoshal rocks in the western part, whereas the central and eastern portions are dominated by extensive granite gneiss. Two major crustal-scale faults, the Son-Narmada North Fault (SNNF) and Son-Narmada South Fault (SNSF), offset the basement and act as important structural boundaries separating different lithological domains. Between these faults, several high-density and high-susceptibility bodies, including Metabasics/Ultrabasic/BIF, Parsoi phyllite/ Ferrogeneous phyllite, greywacke and metabasic-ultramafic intrusions, account for the prominent gravity and magnetic highs. East of the SNSF, Gondwana sediments occupy fault-bounded depressions, while a shallow basalt/ultramafic body near the eastern end explains the localized magnetic high. Overall, the model indicates that the observed geophysical anomalies are primarily controlled by basement architecture, lithological density and susceptibility contrasts, and fault-controlled emplacement of mafic-ultramafic bodies, highlighting the structurally disturbed zone between the SNNF and SNSF as the most prospective domain for concealed mineralisation.

6. Discussion

The integrated interpretation of gravity and magnetic data provides a coherent understanding of the litho-structural framework of the eastern Son Valley region. The Bouguer anomaly (BA) pattern reveals a structurally segmented crust characterised by alternating high- and low-density domains aligned predominantly along ENE–WSW to E–W trends, consistent with the regional tectonic grain of the Son–Narmada Lineament (SNL) system. High gravity anomalies over the Mahakoshal belt indicate the presence of dense lithologies, such as banded iron formations (BIF) and mafic–ultramafic intrusions, suggesting basement uplift or horst-like structures. In contrast, low gravity anomalies associated with the Vindhyan and Gondwana sequences reflect thick accumulations of low-density sediments within structurally controlled basins, indicative of graben-like settings. Derivative-based analyses (THDR, first vertical derivative, analytic signal, and tilt angle) consistently delineate major structural discontinuities,

including the Son–Narmada North Fault (SNNF), Son–Narmada South Fault (SNSF), and the Jiawan–Amsi Fault. The strong spatial correlation of these features across multiple filtering techniques enhances confidence in their interpretation as deep-seated tectonic structures. Furthermore, their persistence in upward-continued gravity fields suggests that these structures extend to significant crustal depths and represent fundamental tectonic boundaries rather than shallow discontinuities.

Magnetic data complement the gravity interpretation by constraining variations in magnetic susceptibility. The reduction-to-pole (RTP) transformation effectively centres anomalies over their causative sources and reveals a prominent E–W trending magnetic high over the Mahakoshal belt, attributed to magnetite-rich lithologies. In contrast, the Vindhyan and Gondwana basins exhibit weak magnetic responses, consistent with their sedimentary composition. Localized magnetic lows within the Mahakoshal terrain are interpreted as zones of demagnetization associated with shearing, indicating structurally altered regions that may facilitate hydrothermal fluid flow. The integration of magnetic derivatives further refines the structural framework. Analytic signal maxima and tilt angle zero contours delineate lithological boundaries and fault zones with high precision, while first vertical derivative maps enhance shallow structural features. The correspondence between gravity- and magnetic-derived lineaments indicates a unified structural architecture dominated by E–W to ENE–WSW trends with subordinate NE–SW and NW–SE orientations, reflecting a polyphase tectonic evolution.

Depth estimation using Euler deconvolution and radially averaged power spectrum (RAPS) analysis provides quantitative constraints on subsurface geometry. The identification of multiple depth levels (~1 km, ~2.5–3 km, and ~8 km) indicates a vertically stratified crust. The intermediate depth (~2.5–3 km), consistently observed in both gravity and magnetic datasets, is interpreted as the basement interface. The deeper gravity-derived interface (~8 km), lacking a corresponding magnetic signature, suggests a relatively non-magnetic lower crust.

The integrated interpretation of gravity and magnetic data, supported by derivative analysis, PDepth solutions, and 2D GM-SYS modelling, provides a coherent understanding of the subsurface architecture and tectonic evolution of the Eastern Son Basin. The derivative maps and depth estimates reveal that the Son–Narmada North Fault (SNNF), Son–Narmada South Fault (SNSF), and associated subsidiary faults constitute deep-seated crustal-scale structural corridors that control basement segmentation, lithological contacts, magmatic emplacement, and basin development. Gravity-derived depth solutions extending to >8 km indicate basement-controlled density interfaces, whereas comparatively shallower magnetic sources (~2 km) correspond to mafic-ultramafic intrusions, BIF horizons, and dyke-like bodies emplaced within the upper crust. The GM-SYS model further confirms that the prominent gravity and magnetic highs are primarily generated by dense and highly magnetic metabasic, ultramafic, and BIF bodies emplaced within the Mahakoshal between the SNNF and SNSF, while Gondwana sediments occupy fault-controlled depressions developed during tectonic reactivation. The spatial coincidence of deep-rooted faults, high-density and high-susceptibility bodies, and strong geophysical anomalies suggests that repeated tectono-magmatic activity localized magma ascent and hydrothermal fluid circulation along these structural corridors. Consequently, the structurally disturbed zone bounded by the SNNF and SNSF represents the most favourable target for concealed mineralisation, demonstrating the effectiveness of integrated gravity and magnetic modelling for mineral exploration beneath sedimentary cover.

From a mineral exploration perspective, the results emphasize the role of structural controls in localizing mineralization. Major fault zones (SNNF, SNSF) and their intersections with subsidiary structures represent zones of enhanced permeability, favourable for fluid migration and ore deposition. The Mahakoshal belt, characterized by high-density and high-susceptibility anomalies, constitutes a prospective zone for iron and associated base-metal mineralization. Additionally, zones of magnetic demagnetization within structurally deformed regions may indicate hydrothermal alteration, further enhancing their exploration significance. The integrated analysis of Bouguer anomaly (BA) and magnetic anomaly (MA) datasets has delineated seven prospective blocks within the study area. These blocks are characterized by distinct geophysical signatures, including residual gravity highs, high-amplitude analytic signal responses, and the convergence of gravity and magnetic lineaments, which collectively

indicate zones of structurally controlled mineralization (Fig. 6). The details of these prospective blocks are described below.

Block	**Gravity Signature**	**Analytic Signal Character**	**Structural Control**	**Geological Interpretation**	**Exploration Priority**
Block-A	Gradient zone	Localized High	Near lineament	Contact-controlled mineralization	Moderate
Block-B	RL–RH transition	Localized High	Near lineament	Deep-seated mineralization	Low–Moderate
Block-C	Strong RH anomaly	Very high amplitude	Major lineament intersection	BIF / Fe ore / intrusive bodies	Very High
Block-D	Localized RH	Localized High	Within structural corridor	Offset mineral system	Very High
Block-E	Moderate linear RH	Elongated AS trend	ENE–WSW structure	Structure controlled mineralization	High
Block-F	Gravity gradient	Moderate MA	E–W and ENE–WSW lineaments (F3–F4)	Ideal shear-hosted hydrothermal setting	High
Block-G	Moderate–High RH	Broad AS highs	Basin margin and lineament	Intrusive / basement-controlled	Moderate–High

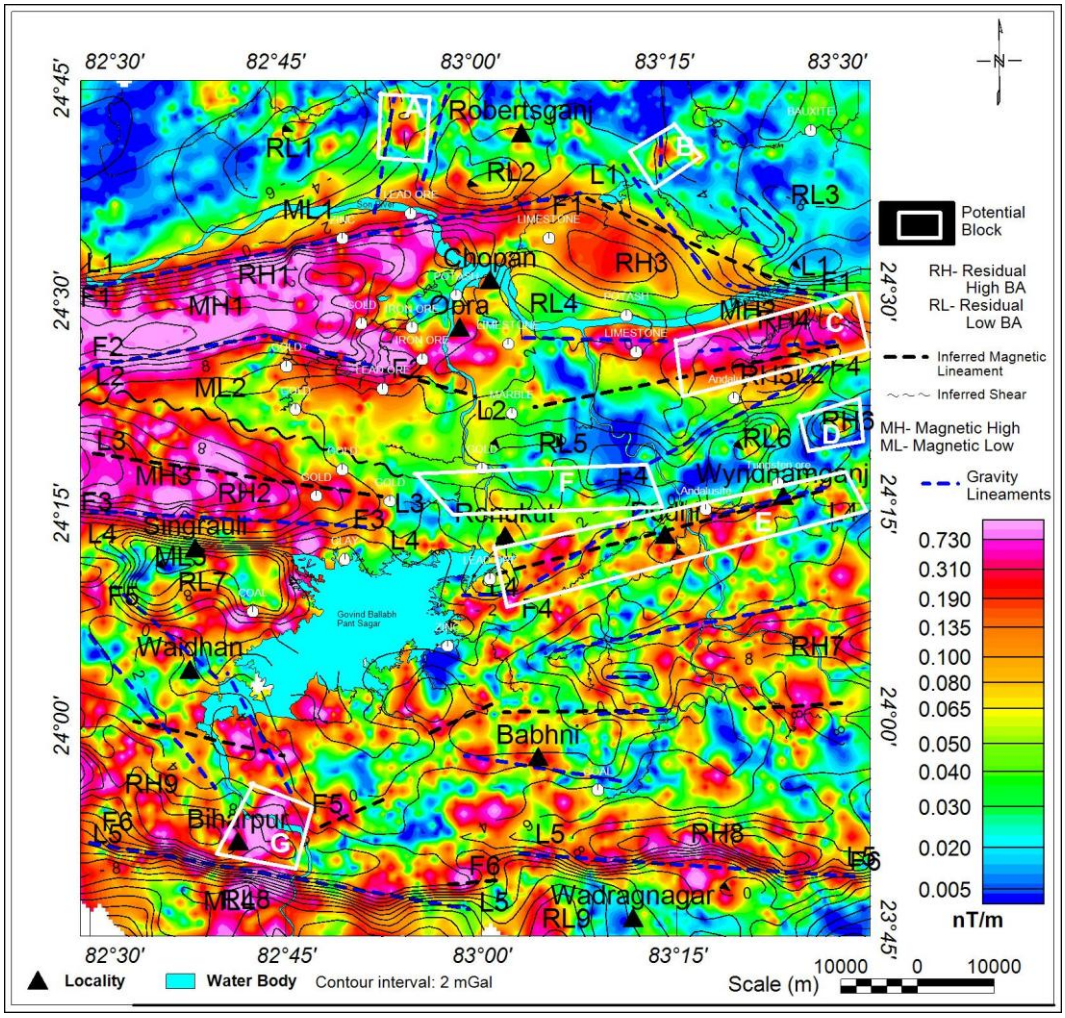


Figure 6: Identified prospective blocks (white box) overlaid on magnetic analytic signal map of the study area.

The geophysical expression of gold mineralization in the study area is primarily governed by structurally controlled hydrothermal processes rather than direct density or magnetic contrasts. Gold occurrences are spatially associated with gravity gradient zones and moderate-to-low magnetic signatures, particularly along major fault and shear systems trending E–W to ENE–WSW. Overall, the integrated analysis demonstrates that the Son Valley region is a structurally controlled domain where deep-seated lineaments govern both basin development and mineralisation. The strong correlation between gravity and magnetic signatures, supported by derivative and depth analyses, provides a robust framework for understanding crustal architecture and identifying prospective mineral zones.

7. Conclusion

This study demonstrates the effectiveness of integrated gravity and magnetic analysis in delineating the litho-structural framework and mineralization potential of the eastern Son Valley region. The Bouguer anomaly pattern reveals a structurally segmented crust characterized by alternating high- and low-density domains aligned along ENE–WSW to E–W trends. High gravity anomalies over the Mahakoshal belt are attributed to dense lithologies, including banded iron formations and mafic–ultramafic rocks, indicating basement uplift. In contrast, low gravity anomalies over the Vindhyan and Gondwana sequences reflect thick accumulations of low-density sediments within fault-controlled basins.

Derivative-based techniques (THDR, first vertical derivative, analytic signal, and tilt angle) effectively delineate major structural features, including the Son–Narmada North and South Faults and associated lineaments. Their persistence in upward-continued fields indicates deep-seated tectonic controls. Magnetic data further constrain lithological variations, with RTP-transformed anomalies highlighting magnetite-rich zones in the Mahakoshal belt and weakly magnetic sedimentary basins. Localized

magnetic lows within the Mahakoshal terrain are interpreted as zones of demagnetization associated with shearing and alteration.

Depth estimates from Euler deconvolution and spectral analysis indicate a vertically stratified crust with interfaces at ~1 km, ~2.5–3 km, and ~8 km, constraining shallow structures, basement configuration, and deeper crustal boundaries.

The integrated analysis of gravity and magnetic data, including derivative techniques, PDepth estimation, and 2.5D GM-SYS modelling, successfully delineated the subsurface geological framework of the Eastern Son Basin. The study identified the Son–Narmada North Fault (SNNF) and Son–Narmada South Fault (SNSF) as major crustal-scale structures controlling basement configuration, magmatic emplacement, and Gondwana basin development. Dense and highly magnetic metabasic, ultramafic, and BIF bodies emplaced within the granitic basement account for the prominent geophysical anomalies. The structurally disturbed corridor between the SNNF and SNSF, characterized by coincident gravity and magnetic highs, is interpreted as the most prospective zone for concealed mineralisation, demonstrating the effectiveness of integrated potential field modelling in mineral exploration.

The results highlight that mineralisation is structurally controlled, with major fault zones and their intersections acting as favourable sites for fluid migration and ore deposition. The Mahakoshal belt represents a key exploration target for iron and associated base metals. Overall, the integrated approach provides a reliable framework for subsurface characterization and mineral exploration in the study area.

Based on the integrated geophysical characteristics and structural analysis, seven prospective target zones (Blocks A–G) have been delineated for future mineral exploration. These targets are defined by the spatial coincidence of residual gravity anomalies, high-amplitude analytic magnetic responses, and structurally significant gravity and magnetic lineaments, indicating zones of structurally controlled mineralization. Further investigation of these targets is recommended through detailed ground-based geophysical surveys, including gravity, magnetic, Induced Polarization (IP), and magnetotelluric (MT) methods. In addition, the application of advanced 3D modelling and inversion techniques is essential to improve subsurface characterization and support more effective and sustainable mineral exploration and resource development.

Data availability

Data will be made available on request.

Authorship contribution statement

Gautam Kumar: Writing – original draft, Software, Methodology, Formal analysis, Data curation, Conceptualization. **Tashmeet Kaur:** Writing–editing, Software, Methodology. **Apratim Kumar Rai:** Software, Formal analysis, Data curation. **Shahina Siddiqui:** Writing, Software, Formal analysis, Data curation. **Resmi Sathikumar:** Software, Formal analysis, Data curation, ***Utkarsh Tripathi*:** Supervision

Acknowledgements

The authors are grateful to the Ministry of Mines and DG, GSI for disseminating the geoscience datasets in the public domain via National Geoscience Data Repository Portal (www.geodataindia.gov.in). The authors thank the ADG & HoD, Geological Survey of India, Lucknow for providing logistics and infrastructure support to carry out this work. They are indebted to all the field officers who are involved in data acquisition during the field work.

Declaration of competing interest

The authors declare that they have no known competing financial interests or personal relationships that could have appeared to influence the work reported in this paper.

Abraham, E.M., Uwaezuoke, A.E., Usman, A.O., 2024. Geophysical investigation of subsurface mineral potentials in North–Central Nigeria: implications for sustainable mining and development. *Geomechanics and Geophysics for Geo-Energy and Geo-Resources* 10, 192. https://doi.org/10.1007/s40948-024-00913-3

Alhassan, A., Aliyu, A., Abdulhameed, Y., Bala, N., Hussaini, A., 2021. Comparison between second vertical derivative and tilt angle methods in detecting edges of gravity anomaly. *Iconic Research and Engineering Journals* 5, 83–87.

Baranov, V., 1957. A new method for interpretation of aeromagnetic maps: pseudo-gravimetric anomalies. *Geophysics* 22 (2), 359–383.

Blakely, R.J., 1996. *Potential Theory in Gravity and Magnetic Applications*. Cambridge University Press, Cambridge.

Choubey, V.M., Kumar, N., Mishra, D.C., 1999. Gravity and magnetic studies over the Vindhyan Basin and their tectonic implications. *Journal of the Geological Society of India* 53, 449–458.

Cooper, G.R.J., Cowan, D.R., 2004. Filtering using variable order vertical derivatives. *Computers & Geosciences* 30 (5), 455–459.

Cooper, G.R.J., Cowan, D.R., 2008. Edge enhancement of potential-field data using normalized statistics. *Geophysics* 73 (3), H1–H4.

Cordell, L., Grauch, V.J.S., Hinze, W.J., 1985. The utility of regional gravity and magnetic anomaly maps. In: *The Utility of Regional Gravity and Magnetic Anomaly Maps*. SEG, pp. 181–197.

Fedi, M., Florio, G., 2001. Detection of potential field source boundaries by the enhanced horizontal derivative method. *Geophysical Prospecting* 49 (1), 40–58.

Ferreira, F.J., de Souza, J., de Bongiolo, A.B.S., de Castro, L.G., 2013. Enhancement of the total horizontal gradient of magnetic anomalies using the tilt angle. *Geophysics* 78 (3), J33–J41.

Geological Survey of India (GSI), 2006. *District Resource Map Series (DRMS), Sonbhadra District, Uttar Pradesh*. GSI, Kolkata.

Geological Survey of India (GSI), 2011. *Geological and Mineral Map of India (1:2,000,000)*. GSI, Kolkata.

Grant, F.S., West, G.F., 1965. *Interpretation Theory in Applied Geophysics*. McGraw-Hill, New York.

Grauch, V.J.S., Cordell, L., 1987. Limitations of determining density or magnetic boundaries from horizontal gradient data. *Geophysics* 52 (1), 118–121.

Jacobsen, B.H., 1987. A case for upward continuation as a standard separation filter. *Geophysics* 52, 1138–1148.

Kebede, H., Alemu, A., Fisseha, S., 2020. Upward continuation and polynomial trend analysis as a gravity data decomposition: case study, Ziway–Shala basin, Ethiopia. *Heliyon* 6 (1), e03292.

Li, Y., & Oldenburg, D. W. (1996). 3-D inversion of magnetic data. Geophysics, 61(2), 394–408.

Li, Y., & Oldenburg, D. W. (1998). 3-D inversion of gravity data. Geophysics, 63(1), 109–119.

Mahadevan, T.M., 2002. *Geology of Bihar and Jharkhand*. Geological Society of India, Bangalore.

Miller, H.G., Singh, V., 1994. Potential field tilt—a new concept for location of potential field sources. *Journal of Applied Geophysics* 32, 213–217.

Misra, P.S., Singh, V., Tripathi, U., Ahmed, S., Bage, G., Tiwari, C.B., Saha, S.K., 2023. Gold mineralisation in eastern Mahakoshal belt of central India: a reappraisal based on mineral system. *Journal of the Geological Society of India* 97 (9), 985–992.

Mishra, D.C., Ravi Shankar, Singh, B., 2000. Crustal structure of central India from gravity and magnetic studies. *Journal of the Geological Society of India* 55, 45–60.

Mishra, D.C., Pedersen, L.B., 1982. Statistical analysis of potential fields from surface relief. *Geoexploration* 19, 247–265.

Nabighian, M. N., 1972, "The Analytic Signal of Two-Dimensional Magnetic Bodies with Polygonal Cross-Section: Its Properties and Use for Automated Anomaly Interpretation", *Geophysics*, vol. 37 (3), pp. 507-517.

Nabighian, M. N., 1974, "Additional Comments on the Analytic Signal of Two-Dimensional Magnetic Bodies with Polygonal Cross-Section", *Geophysics*, vol. 39 (1), pp. 85-92.

Naqvi, S.M., Rogers, J.J.W., 1987. *Precambrian Geology of India*. Oxford University Press, New York.

Nishijima, J., Naritomi, K., 2017. Interpretation of gravity data to delineate underground structure in the Beppu geothermal field, Japan. *Journal of Hydrology: Regional Studies* 11, 84–95.

Phillips, J. D., 1997, "Potential-Field Geophysical Software for the PC, version 2.2", *USGS*, Open-File Report 97-725, desc. 39 p.

Pilkington, M., Keating, P., 2004. Contact mapping from gridded magnetic data: a comparison of techniques. *Exploration Geophysics* 35 (4), 306–311.

Ramakrishnan, M., Vaidyanadhan, R., 2010. *Geology of India*, vols. 1–2. Geological Society of India, Bangalore.

Ravat, D., Kirkham, K., Hildenbrand, T.G., 2002. A source-depth separation filter using Euler method. *The Leading Edge* 21 (4), 360–365.

Reid, A.B., Allsop, J.M., Granser, H., Millett, A.J., Somerton, I.W., 1990. Magnetic interpretation in three dimensions using Euler deconvolution. *Geophysics* 55 (1), 80–91.

Roest, W.R., Verhoef, J., Pilkington, M., 1992. Magnetic interpretation using the 3-D analytic signal. *Geophysics* 57 (1), 116–125.

Rosid, M.S., Siregar, H., 2017. Determining fault structure method: a comparative study. *AIP Conference Proceedings* 1862, 030171.

Ravi Shankar, 1991. Geophysical significance of the Narmada–Son Lineament. *Journal of the Geological Society of India* 38, 211–220.

Saha, D., Deb, M., Mukherjee, B.K., 2011. Gold mineralization in the Mahakoshal belt: geological and structural controls. *Ore Geology Reviews* 39, 186–200.

Saltus, R. W., & Blakely, R. J. (2011). Unique geologic insights from "non-unique" gravity and magnetic interpretation. GSA Today, 21(12), 4–10. https://doi.org/10.1130/G136A.1

Spector, A., Grant, F.S., 1970. Statistical models for interpreting aeromagnetic data. *Geophysics* 35, 293–302.

Srivastava, R.K., 2012. Precambrian geology of central India: petrological and tectonic evolution. *Journal of Earth System Science* 121 (5), 1203–1220.

Talwani, M., Worzel, J.L., Landisman, M., 1959. Rapid gravity computations for two- dimensional bodies with application to the Mendocino submarine fracture zone. J. Geophys. Res. 64, 49–59. doi: 10.1029/JZ064i0 01p0 0 049 .

Talwani, M., Heirtzler, J.R., 1964. Computation of magnetic anomalies caused by two-dimensional bodies of arbitrary shape. Geophysics 9, 464–480.

Telford, W.M., Geldart, L.P., Sheriff, R.E., 1990. *Applied Geophysics*, 2nd ed. Cambridge University Press, Cambridge.

Thompson, D.T., 1982. EULDPH: a new technique for depth estimation from magnetic data. *Geophysics* 47, 31–37.

Tiwari, V.M., Mishra, D.C., Singh, B., 2001. Gravity studies over central Indian tectonic zones. *Journal of Asian Earth Sciences* 19, 451–460.

Verduzco, B., Fairhead, J.D., Green, C.M., MacKenzie, C., 2004. New insights into magnetic derivatives for structural mapping. *The Leading Edge* 23, 116–119.